Acta Materialia 98 (2015) 416–422

Contents lists available at ScienceDirect

Acta Materialia

journal homepage: www.elsevier.com/locate/actamat

Structure and chemical bonding in $MgNi_2H_3$ from combined high resolution synchrotron and neutron diffraction studies and *ab initio* electronic structure calculations

V.A. Yartys [a,b,*], V.E. Antonov [c,d], D. Chernyshov [e], J.-C. Crivello [f], R.V. Denys [a], V.K. Fedotov [c], M. Gupta [g], V.I. Kulakov [c], M. Latroche [f], D. Sheptyakov [h]

[a] *Institute for Energy Technology, Kjeller, Norway*
[b] *Norwegian University of Science and Technology, Trondheim, Norway*
[c] *Institute of Solid State Physics RAS, 142432 Chernogolovka, Moscow district, Russia*
[d] *National University of Science and Technology 'MISIS', 119049 Moscow, Leninskii prosp. 4, Russia*
[e] *Swiss-Norwegian Beam Lines, ESRF, Grenoble, France*
[f] *Institut de Chimie et des Matériaux Paris-Est, ICMPE-CNRS-UPEC, Thiais, France*
[g] *Institut de Chimie Moléculaire et des Matériaux, ICMMO-CNRS-Université Paris Sud, Orsay, France*
[h] *Laboratory for Neutron Scattering and Imaging, Paul Scherrer Institut, 5232 Villigen PSI, Switzerland*

ARTICLE INFO

Article history:
Received 8 July 2015
Accepted 20 July 2015

Keywords:
Metal hydrides
Crystal structure
High pressures
Neutron diffraction
DFT
Phonon
Magnesium
Nickel

ABSTRACT

Our earlier study Yartys et al. (2015) showed that at high hydrogen pressures, hexagonal $MgNi_2$ undergoes a hydrogen assisted phase transition into the orthorhombic $MoSi_2$-type structure. Here we report on a combined high resolution synchrotron and neutron diffraction investigation of the crystal structure of $MgNi_2D_3$, and *ab initio* calculation of its electronic structure that revealed the nature of the metal–hydrogen bonding. The diffraction data (293 and 1.8 K) are well described with a *Cmca* unit cell with H atoms filling the deformed octahedra Mg_4Ni_2 and the positions within the buckled nets –Ni–H–Ni–H– penetrating through the structure. DFT and phonon calculations showed that the *Cmca* structure of $MgNi_2D_3$ is the most stable, both from the electronic structure and the lattice dynamical arguments. The Bader charge analysis indicates an electronic transfer from Mg ($-1.59e^-$) to Ni ($+0.21e^-$), H1 ($+0.55e^-$) and H2 ($+0.31e^-$). The phonon dispersion curves of $MgNi_2H_3$ show positive frequencies, indicating that the structure is mechanically stable. The calculated gross heat of formation for the *Cmca* phase of $MgNi_2H_3$ is -37.3 kJ/mol-H_2, which makes it more stable by 3 kJ/mol-H_2 than the prototype structures tested in Yartys et al. (2015). The stability of the *Cmca* crystal structure of $MgNi_2H_3$ is enhanced by the formation of the directional Ni–H covalent bonds supplemented by the electron transfer from Mg to both Ni and H. The heat capacity as a function of temperature is obtained by phonon calculation in the quasi-harmonic approximation.

1. Introduction

In our earlier study, we have shown that the hydrogenated $MgNi_2$ intermetallic compound with *C*36 Laves-type structure forms a trihydride $MgNi_2H_3$ and undergoes a hydrogen-induced phase transformation into an orthorhombic $MoSi_2$-type related structure [1]. The hydrogenation was carried out in a hydrogen (deuterium) gas compressed to 2.8–7.4 GPa at 300 °C.

The orthorhombic structure of $MgNi_2D_3$ was studied using time-of-flight neutron scattering in the *d*-spacing range between 1 and 5 Å performed at the Joint Institute for Nuclear Research in Dubna, Russia. These studies showed that hydrogen atoms fill two types of interstices, inside the Mg_4Ni_2 octahedrons and inside the buckled nickel nets [1].

It should be noted, however, that phase transformations in the $MgNi_2$-$H(D)_2$ system are rather complex and can result in the formation of tetragonal and orthorhombic modifications of $MgNi_2H(D)_3$ according to Kataoka and coworkers [2,3]. In this connection, a high resolution powder diffraction investigation of $MgNi_2D_3$ would be of great value in order to improve quality of the raw experimental data and determine the nature of chemical

* Corresponding author at: Institute for Energy Technology, Kjeller, Norway.
E-mail addresses: volodymyr.yartys@ife.no, volodymyr.yartys@gmail.com (V.A. Yartys).

http://dx.doi.org/10.1016/j.actamat.2015.07.053
1359-6454/

bonding stabilizing the formed trihydride and causing the rebuilding of the metal sublattice.

It is well known that intermetallic hydrides demonstrate a close interrelation between their crystal chemistry and hydrogen storage behaviours thus allowing optimization of the H storage performance [4]. Hydrogen accommodation by the metal lattice is typically accompanied by a modest (few percent) increase of the interatomic metal–metal distances, while the H atoms fill the available interstices in the intermetallic structures. However, in a number of cases a formation of the metal hydride leads to rebuilding of the metal sublattice. Such a rebuilding is of particular interest as it could be related to the unconventional metal–hydrogen bonding in the hydrides thus formed. It is exactly the case of the $MgNi_2H_3$ hydride. In this hydride, only small part of the hydrogen atoms fills the interstitial sites available in the structure of the virgin $MgNi_2$ compound, whereas the major part of the H atoms is exclusively bound to the nickel atoms and produce ···H–Ni–H–Ni ··· nets because of the formation of directional, partially covalent Ni–H bonds [1].

The objective of the current study is:

(a) application of combined synchrotron X-ray diffraction and neutron diffraction to the characterization of the crystal structure of $MgNi_2H(D)_3$;
(b) theoretical density functional theory (DFT) and phonon calculations based on the initial high accuracy crystallographic data to describe the nature of the chemical bonding and the thermodynamic properties of the studied hydride.

2. Experimental

2.1. Synthesis of $MgNi_2$ and $MgNi_2D_3$

The starting $MgNi_2$ material was the same as that used in [1] and prepared from high-purity Mg (99.8%) and Ni (99.995%) powders mixed with a slight excess of Mg (2 wt.%) as compared to the stoichiometric ratio Mg:Ni = 1:2. The mixture was compacted by pressing into pellets with a diameter of 15 mm. The pellets were sintered in argon gas at 800 °C for 12 h and quenched into ice water. XRD study showed the formation of a $MgNi_2$ intermetallic compound crystallizing with a Laves type hexagonal $MgNi_2$ type structure (C36) with the unit cell parameters a = 4.82565(6), c = 15.8323(3) Å. This compound constituted about 90 wt.% of the material, the impurities being Ni metal, MgO and $MgNi_3$ compound [1].

A 1000 mg sample of the $MgNi_2$-based deuteride was prepared by a 24 h exposure of the powdered $MgNi_2$ to a D_2 pressure of 2.8 GPa at 300 °C. The sample was prepared in 5 batches, each containing appr. 200 mg of the material. Before releasing the pressure, the synthesized deuteride was rapidly cooled (quenched) to 100 K. The hydrogenation method is described in more detail elsewhere [5]. The experiment was carried out in a Toroid-type high-pressure chamber [6] using AlD_3 as an internal deuterium source.

In agreement with results of [1] for the $MgNi_2$-D sample prepared in the same way, our quenched sample consisted of the orthorhombic $MgNi_2D_3$ phase with admixture of MgO and NiD deuteride; the latter was formed from the impurities of Ni and $MgNi_3$ contained in the starting material. When the quenched sample was further heated to room temperature, the NiD phase rapidly decomposed to Ni metal and D_2 gas, while the $MgNi_2D_3$ phase did not lose deuterium for a week at least.

In the present work, we examined the $MgNi_2$-D sample composed of all 5 synthesized batches mixed together and powdered in an agate mortar in an Ar glove box. The resulting powder sample was exposed to room temperature and pressure in an Ar atmosphere for a few days needed for the sample transportation between our institutions. Rest of the time the sample was stored in liquid nitrogen to prevent the deuterium loss and oxidation by air.

2.2. Synchrotron X-ray diffraction

The study was performed at the beam station BM1A at the Swiss-Norwegian Beam Lines, European Synchrotron Research Facility, Grenoble, France, using a multipurpose diffractometer based on the PILATUS2 M detector. The data were collected at 293 K using monochromatic X-ray beam with a wavelength of 0.68894(1) Å in the 2θ range 2.5–73.2°; step size 0.021748°. The wavelength was calibrated by collecting the data for a standard sample of LaB_6 (NIST standard). The measured $MgNi_2D_3$ sample was enclosed in a sealed glass capillary with a diameter of 0.3 mm.

2.3. Neutron powder diffraction (NPD)

The $MgNi_2D_3$ deuteride was studied by neutron diffraction at the Spallation Neutron Source SINQ at Paul Scherrer Institute, Villigen, Switzerland, using a high resolution powder diffractometer HRPT in the high intensity mode (λ = 1.494 Å, 2θ range 4.5–164.7°, step 0.05°). The sample with the overall mass of 1 g was placed into a 6 mm vanadium sample holder. Loading the deuteride into the sample holder was performed in an argon glove box.

Two data sets were measured, at 293 K and at 2 K. The latter dataset was collected on a sample placed into a standard orange cryostat.

2.4. Combined SR XRD and NPD Rietveld profile refinements

Combined Rietveld refinements of the neutron and synchrotron powder diffraction data collected at 293 K and at 2 K were performed using the GSAS software [7].

2.5. Electronic structure calculations

The calculations are based on the density functional theory (DFT) and performed in the same conditions (method, accuracy) as in the previous study [1]. We use the projector augmented wave method (PAW) [8] implemented in the Vienna *Ab initio* Simulation Package (VASP) [9,10] with the Perdew–Burke–Ernzerhof exchange–correlation functional [11] including semi-core *p* electrons of Mg and Ni. After the necessary tests to control the stability of the energy differences between the phases, the energy cut-off for the PAWs was set to 800 eV. Phonon calculations are carried out in the harmonic (HA) and quasi-harmonic (QHA) approximation [12] from the supercell approach ($2 \times 1 \times 2$: 96 atoms) with the finite displacement method [13] using the Phonopy code [14]. Charge transfers are computed using Bader's prescription [15,16].

3. Results and discussion

3.1. Thermal stability of $MgNi_2D_3$

The thermal stability and the total hydrogen content of the sample were studied by deuterium desorption in the temperature range 15–350 °C in the regime of heating at a rate of 2 °C/min in a closed-volume, pre-evacuated measuring system. In this experiment, we used a portion of the sample with a mass of 150 mg. The initial pressure in the system was near 0 bar, and the final pressure was 2.97 bar. The results are shown in Fig. 1.

As seen from Fig. 1, the total amount of deuterium released from the $MgNi_2$-D sample reached 3.6 wt.% with a peak of

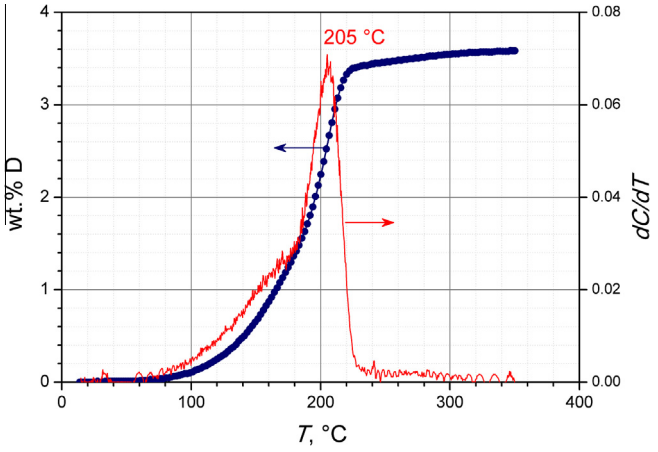

Fig. 1. Thermal desorption traces of deuterium release from the $MgNi_2D_{2.93}$ sample pre-exposed to ambient conditions for a few days.

deuterium desorption at appr. 205 °C. According to the synchrotron XRD investigation (see Section 3.2), the sample was composed of about 90 wt.% $MgNi_2D_{\sim 3}$. Two impurity phases (total content ~10 wt.%) were identified as MgO and Ni containing no deuterium. Consequently, the $MgNi_2D_{\sim 3}$ deuteride contained 3.6/0.9 = 4.0 wt.% D that corresponds to the stoichiometry $MgNi_2D_{2.93}$.

3.2. Synchrotron X-ray diffraction study

In agreement with our earlier study [1], the refinements of the SR XRD pattern concluded that $MgNi_2D_3$ crystallises with orthorhombic structure. The refinements indicated presence of two impurity phases, nickel and magnesium oxide (both coming from the original alloy).

However, the refinements also showed that the *Fmmm* space group (S.G.) proposed in [1] does not allow one to describe all observed reflections. The strongest extra peaks are marked by arrows in Fig. 2. We have tried several other space groups with a lower symmetry, including the *Pmmm* space group proposed in [2,3]. These refinements did not provide satisfactory improvements. The observed extinctions of the Bragg indexes of the strongest resolved extra peaks (0 2 1, 2 2 1 and 1 3 2) suggested that the structure has a *C* centred orthorhombic unit cell instead of the *F* type cell.

One of the possible space groups is *Cmca* (No. 64), which is related to the S.G. *Fmmm* via the group-subgroup relations [*Fmmm* (No. 69) → *Cmca* (No. 64; setting 1): $a \rightarrow a$; $b \rightarrow c$; $c \rightarrow b$]. This group provided an excellent description of the observed diffraction pattern (see the fit of the SR XRD pattern in Fig. 2). Consequently, the *Cmca* space group was used in the profile analysis of the neutron powder diffraction patterns.

3.3. Neutron powder diffraction study at 293 K

During the deuteration, the $MgNi_2$ compound underwent a volumetric expansion of 15.6%, from $V(MgNi_2)$ = 319.291/8 = 39.91 Å^3/f.u. to $V(MgNi_2D_3)$ = 189.17/4 = 47.29 Å^3/f.u.

The NPD data collected at 293 K were refined together with the SR XRD data discussed in Section 3.2. The refinement showed excellent agreement between the experimental and calculated patterns (Fig. 3). Crystal structure data for the $MgNi_2D_3$ deuteride are given in Table 1.

In the structure of $MgNi_2D(H)_3$ hydrogen atoms occupy two types of sites, (a) inside the deformed octahedra Mg_4Ni_2 and (b) within the buckled nets –Ni–H–Ni–H– containing infinite bended spirals penetrating through the structure. This is schematically shown in Fig. 4. As is also seen from Fig. 4, the D2 position of the deuterium atoms has chair coordination by the neighbouring Ni atoms.

Fig. 5 compares the *Fmmm* and *Cmca* structures of $MgNi_2H(D)_3$. As one can see, both the Mg_4Ni_2 octahedra and buckled networks ···Ni–H2–Ni–H2··· undergo a significant deformation in the *Cmca* structure. This deformation makes the *Cmca* structure more thermodynamically favourable than *Fmmm*.

The bonding Me–H(D) distances in the *Cmca* structure are: D1–Ni 1.6213(5) Å; D1–Mg 2.2951(1) Å; D1–Mg 2.3431(1) Å; D2–Ni 1.7444(4) Å; D2–Ni 1.7947(4) Å. These distances well agree with the average Mg–H and Ni–H separations observed in the structures of binary and ternary hydrides. As an example, consider 1.97–2.17 Å for the Mg–H and 1.52–1.74 Å for the Ni–H distances in $La_2MgNi_9D_{13}$ deuteride [17].

The shortest D–D separations in the structure are in agreement with the "rule of 2 Å" [4]; D2–D2: 2.295 Å and 2.402 Å; D1–D2: 2.536 Å.

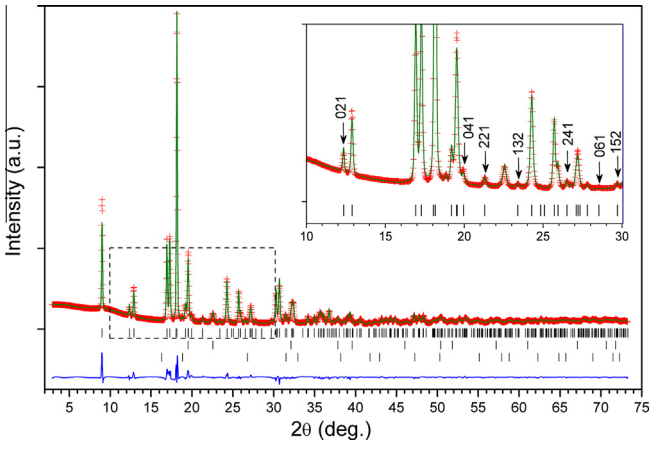

Fig. 2. SR XRD pattern (λ = 0.68894 Å) of $MgNi_2D_3$ at 293 K used in the combined refinements of the SR XRD and NPD patterns. R_p = 5.5%, R_{wp} = 5.7%, R_{F^2} = 3.4. Vertical bars show positions of the Bragg peaks for the phase constituents (from top to bottom): $MgNi_2D_3$ (90.9%); Ni (7.6%); MgO (1.5%). Crosses represent the experimental data, solid lines are for the calculated profile and difference plot. Inset: strongest extra peaks and their *hkl* indexes.

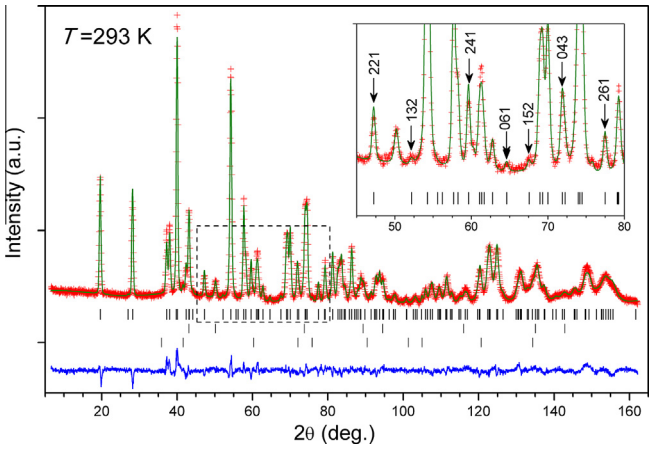

Fig. 3. NPD pattern (λ = 1.494 Å) of $MgNi_2D_3$ at 293 K used in the combined refinements of the SR XRD and NPD pattern. NPD: R_p = 3.7%, R_{wp} = 4.9%, R_{F^2} = 4.4. Vertical bars show positions of the Bragg peaks for the phase constituents (from top to bottom): $MgNi_2D_3$ (90.9%); Ni (7.6%); MgO (1.5%). Crosses represent the experimental data, solid lines are for the calculated profile and difference plot. Inset: strongest extra peaks and their *hkl* indexes.

Table 1
Crystal structure data for the deuteride $MgNi_2D_3$ at 293 K from the combined refinements of the SR XRD and NPD data and from the theoretical calculations. Sp.gr. *Cmca* (No. 64). Experimental data: $a = 4.5902(1)$; $b = 8.7943(2)$; $c = 4.6861(1)$ Å; $V = 189.17(1)$ Å^3. Theoretical calculations: sp.gr. *Cmca* (No. 64). $a = 4.5356$; $b = 8.8407$; $c = 4.6938$ Å; $V = 188.21$ Å^3.

Atom	Wyckoff site	Experimental results				Theoretical calculations		
		x	*y*	*z*	$U_{iso} \times 100$ (Å^2)	*x*	*y*	*z*
Mg	4*a*	0	0	0	0.65(3)	0	0	0
Ni	8*f*	0	0.3167(1)	0.0363(1)	0.30(1)	0	0.3154	0.0478
D1	4*b*	½	0	0	2.7(1)	½	0	0
D2	8*e*	¼	0.2199(2)	1/4	2.7(1)	¼	0.2143	¼

Site occupancy factors for all atoms were fixed to 1.0 and not refined. Phase fractions: $MgNi_2D_3$ – 90.9(1) wt.%; Ni (*Fm*$\bar{3}$*m* $a = 3.5265(1)$ Å)–7.6(1) wt.%; MgO (*Fm*$\bar{3}$*m*; $a = 4.2135(6)$ Å)–1.5(1) wt.%.

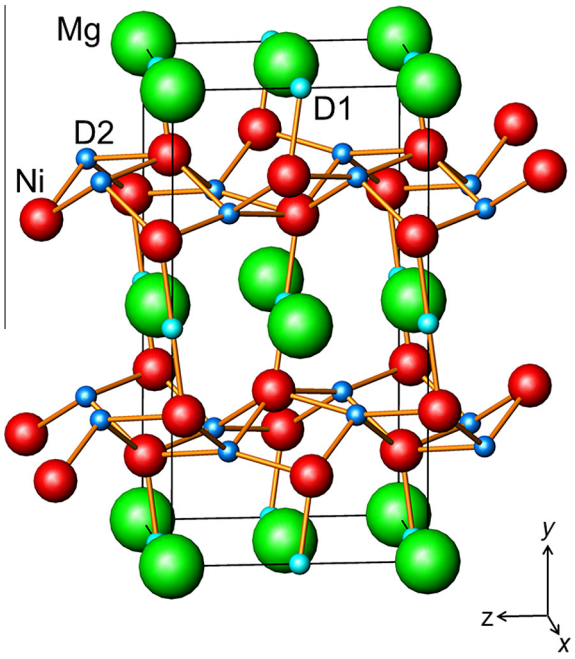

Fig. 4. Crystal structure of $MgNi_2D_3$. Two types of sites occupied by deuterium include a Mg_4Ni_2 octahedron for H1(D1) and a chair Ni_4 configuration for H2(D2) located within the buckled Ni–H nets containing bended spirals –Ni–H2–Ni–H2–.

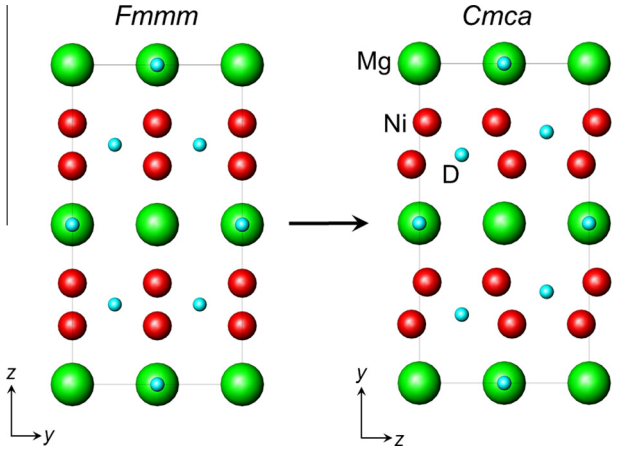

Fig. 5. Relationship between the crystal structures of $MgNi_2D_3$ in the space group *Fmmm* [1] and in the space group *Cmca* (present study).

3.4. Neutron powder diffraction study at 2 K

Crystal structure data for $MgNi_2D_3$ were also collected at 2 K (neutron powder diffraction study only). This study showed that the cooling of the sample from 293 to 2 K is accompanied by a small contraction of the unit cell slightly exceeding 1% in total. Interestingly, this contraction is very anisotropic and is confined to the [100] direction only. Indeed, $\Delta a/a_{RT} = -1.18\%$; $\Delta b/b_{RT} = -0.05\%$; $\Delta c/c_{RT} = -0.01\%$; $\Delta V/V_{RT} = -1.25\%$.

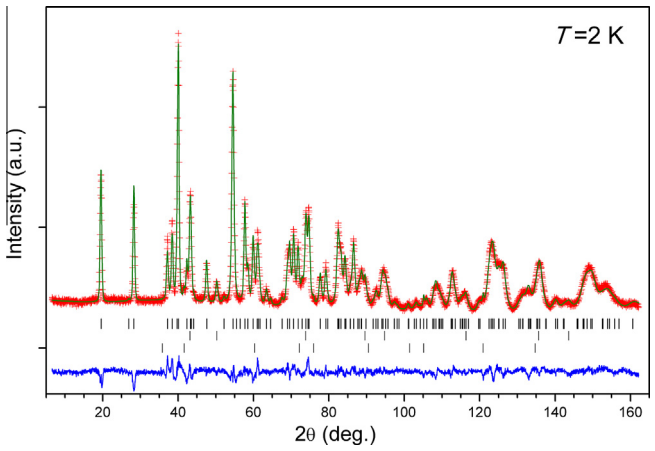

Fig. 6. NPD pattern ($\lambda = 1.494$ Å) of $MgNi_2D_3$ at 2 K. $R_p = 3.8\%$, $R_{wp} = 4.8\%$, $R_{F^2} = 3.2$. Vertical bars show positions of the Bragg peaks for the phase constituents (from top to bottom): $MgNi_2D_3$ (91.9%); Ni (6.8%); MgO (1.3%). Crosses represent the experimental data, solid lines are for the calculated profile and ~~a~~ difference plot.

The NPD pattern of $MgNi_2D_3$ collected at 2 K is shown in Fig. 6. Results of the refinements of the crystal structure of $MgNi_2D_3$ at 2 K are summarized in Table 2. The bonding Me–H(D) distances in this structure show only minor changes due to the cooling from 293 to 2 K and attain the following values: D1–Ni 1.6336(9) Å; D1–Mg 2.2680(1) Å; D1–Mg 2.3428(1) Å; D2–Ni 1.732(4) Å; D2–Ni 1.8094(9) Å.

3.5. DFT calculations of the electronic structure of $MgNi_2H_3$

Starting with the crystal structure data experimentally determined in the present study, the theoretical calculations allowing a full relaxation of the unit cell led to a symmetry converged to the base centred orthorhombic *Cmca* space group (S.G. No. 64), with very comparable values of the cell parameters and internal positions to those from the experiments, see Table 1. One may notice that the *Cmca* space group and the monoclinic *C*2/*m* group (S.G. No. 12) resulting from *ab initio* calculations [1], are both maximal non-isomorphic subgroups of the *Fmmm* (S.G. No. 69) symmetry proposed for the $MgNi_2H_3$ phase on the experimental basis [1].

Since the atomic environments are very similar, the electronic density of states (DOS) of $MgNi_2H_3$ calculated in the *Cmca* S.G. and shown in Fig. 7, is very similar to the DOS in the *Fmmm* S.G. (shown in Fig. 10 of Ref. [1]). Thus, the discussion is intentionally omitted and we suggest reading the Section 3.5.2 of [1] for

Table 2
Crystal structure data for $MgNi_2D_3$ at 2 K. Sp.gr. *Cmca*, $a = 4.5360(2)$, $b = 8.7895(4)$, $c = 4.6857(2)$ Å; $V = 186.81(2)$ Å^3.

Atom	Wyckoff site	*x*	*y*	*z*	$U_{iso} \times 100$ (Å^2)
Mg	4*a*	0	0	0	0.0(–)
Ni	8*f*	0	0.3157(1)	0.0456(2)	0.0(–)
D1	4*b*	1/2	0	0	1.5(1)*
D2	8*e*	1/4	0.2143(2)	1/4	1.6(1)*

Phase fractions: $MgNi_2D_3$ – 91.9(1) wt.%; Ni ($Fm\bar{3}m$; $a = 3.5160(3)$ Å)–6.8(1) wt.%; MgO ($Fm\bar{3}m$; $a = 4.206(1)$ Å)–1.3(1) wt.%. Site occupancy factors for all atoms were fixed to 1.0.

* Atomic displacement parameters.

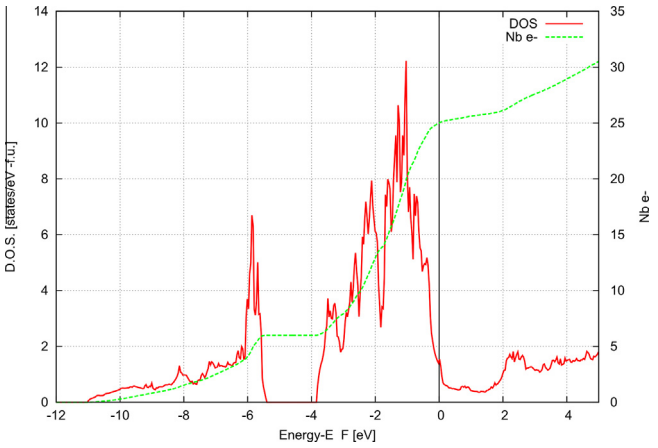

Fig. 7. Total electronic DOS of the *Cmca* phase of $MgNi_2H_3$ (left vertical scale) and the number of its electrons (right vertical scale). The Fermi level is chosen as the origin of the energies.

complementary details. The directional Ni–H covalent bonds associated with short Ni–H distances are supplemented, as in [1], by an electron transfer from Mg to H and Ni atoms. The Bader charge analysis is also similar and predicts an electronic transfer from Mg ($-1.59e^-$) to Ni ($+0.21e^-$), H1 ($+0.55e^-$) and H2 ($+0.31e^-$). The large difference in the charge transfer between H1 and H2 is due to their different local environment: as one can see from Fig. 4, H1 is surrounded by 2 Ni and 4 Mg atoms, while the first nearest neighbours of H2 are Ni atoms, the Mg atoms being more distant neighbours.

Concerning the $MgNi_2 + 3/2\ H_2 \rightarrow MgNi_2H_3$ reaction, the DFT and phonon calculations of all products and reactants allowed us to obtain the energy of reaction and zero-point energy (ZPE). The gross heat of formation of the *Cmca* hydride, without ZPE correction, is $\Delta H = -37.35$ kJ/mol-H_2 that makes this hydride by about 3 kJ/mol more stable than all the prototype structures previously tested in [1]. The ZPE energy contribution is however larger, nevertheless the final ZPE corrected heat of formation is still the lowest in the *Cmca* structure with $\Delta H^{corr} = -27.89$ kJ/mol-H_2. The values obtained in [1] for the *Fmmm* structure are $\Delta H = -34.10$ kJ/mol-H_2 for the gross heat of formation and $\Delta H^{corr} = -26.15$ kJ/mol-H_2 for its ZPE corrected value.

The phonon dispersion curves of $MgNi_2H_3$ calculated in the *Cmca* symmetry are presented in Fig. 8. All frequencies are positive therefore indicating that the structure is mechanically stable. An analysis of the different vibrational contributions can be obtained from the partial phonon DOS shown in Fig. 9. At lower frequencies, the contributions from the heaviest Ni and Mg atoms are dominant with some coupled modes, whereas the contributions at higher frequencies come from the hydrogen vibrations.

The high-energy very localized mode at ≈48.5 THz (1 THz = 4.15 meV) is believed to be determined by the strong interactions of H1 with its 2 Ni first neighbours located at short distances, 1.647 Å in the DFT relaxed structure, while the H2 optic modes located between 21.5 and 35.0 THz, are much softer since the H2 distances to its 4 Ni neighbours are much larger, ranging from 1.728 to 1.818 Å. The high energy localized modes of H1 obtained in the present calculation have frequencies ≈48.5 THz, which are slightly smaller than ≈51 THz calculated in [18] for the low temperature phase of Mg_2NiH_4 and associated with very short Ni–H distances, ≈1.54–1.56 Å, H being in a distorted tetrahedral environment. The lowest H2 frequencies are comparable to the experimental characteristic optic phonon frequencies ≈21.5 THz of $NiH_{1.05}$ [19], where H occupies octahedral interstices

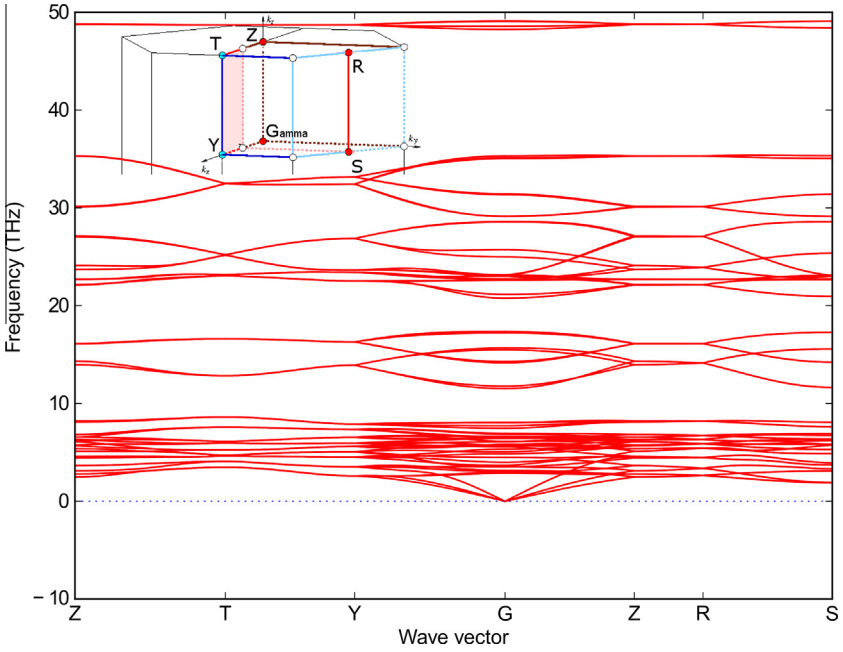

Fig. 8. Phonon dispersion curves of $MgNi_2H_3$ in the *Cmca* space group.

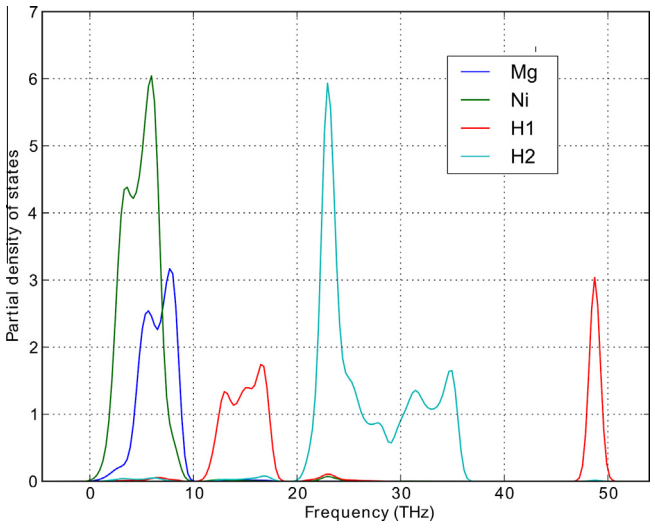

Fig. 9. Partial phonon DOS of $MgNi_2H_3$ in the *Cmca* space group.

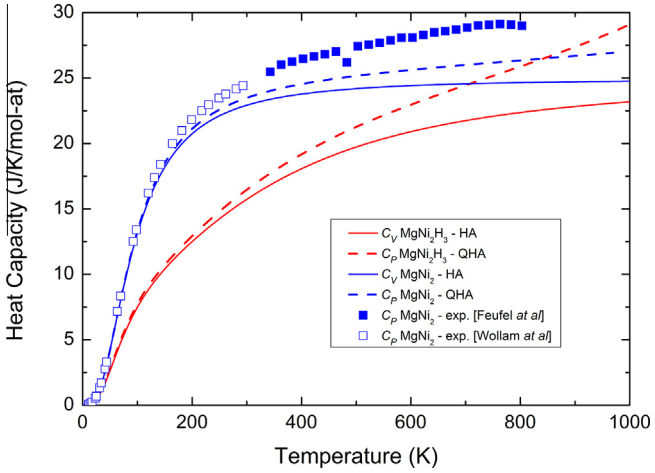

Fig. 10. Heat capacities of $MgNi_2$ and $MgNi_2H_3$ at constant volume (harmonic approximation: HA) and at constant pressure (quasi-harmonic approximation: QHA). Experimental results of C_p measured for $MgNi_2$ are taken from the literature [20,21].

with a Ni–H distance of 1.86 Å. The strong $\vec{q}$ dependence of the H2 optic modes points to significant H-H long range interaction. In the 11.5–17.5 THz range, the H1 vibration modes can be mostly associated with the interaction of H1 with its 4 Mg neighbours in the plane.

The calculated heat capacities of the $MgNi_2$ and $MgNi_2H_3$ compounds at constant volume, C_v, and at constant pressure, C_p, are given in Fig. 10. As expected, the C_p values are enhanced relative to C_v, since $C_p = C_V + \alpha^2 TV/\beta$, where $V(T)$ is the molar volume, $\alpha = (1/V)(\partial V/\partial T)_p$ the thermal coefficient of volume expansion, and $\beta = -(1/V)(\partial V/\partial P)_T$ the isothermal compressibility.

Fig. 11 shows the temperature dependence of the unit cell volume for these compounds calculated in QHA. One can see that the volume of the hydride increases more rapidly at high temperatures. The temperature dependence of the thermal coefficient of volume expansion $\alpha(T)$ *is* also given as a helpful information for the reader. The calculated $C_p(T)$ of $MgNi_2$ agrees with experimental results of Ref. [20] obtained at low and moderate temperatures. The experimental values of C_p measured at higher temperatures in Ref. [21] noticeably differ from our estimates. The discrepancy could be due, in part, to some anharmonic contributions neglected in our calculations, but further experimental confirmation is also desirable. The calculated C_p in the high temperature limit is slightly larger than the $3R$/mol-atom ≈24.9 J/K/mol-atom of the Dulong–Petit law. At low and moderate temperatures, when the high frequency H vibrations are not yet excited, the heat capacity of the hydride $MgNi_2H_3$ on a per atom basis should be lower than that of $MgNi_2$, as found in Fig. 10.

As a conclusion from the theoretical part of the paper, the *Cmca* structure of $MgNi_2H_3$ is shown to be the most stable one from both the electronic and the lattice dynamical arguments, in agreement with the XRD and NPD-2K results.

4. Conclusions

The combined high resolution synchrotron and neutron diffraction studies of $MgNi_2H(D)_3$ showed that during the hydrogenation of the hexagonal Laves type intermetallic compound $MgNi_2$, it transforms into the orthorhombic $MoSi_2$-type structure. Together with the *ab initio* calculation of the electronic structure, these studies revealed the mechanism of the metal–hydrogen bonding in the *Cmca* phase of $MgNi_2H(D)_3$.

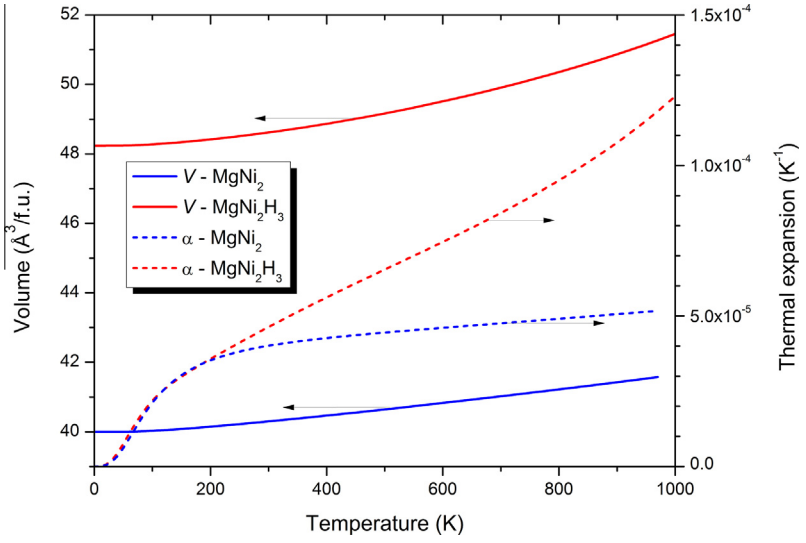

Fig. 11. Unit cell volume (solid curve, left vertical scale) and thermal expansion coefficient (dashed curve, right vertical scale) as a function of temperature calculated for $MgNi_2$ and $MgNi_2H_3$ in the QHA approximation.

The diffraction data collected at 293 and 2 K are perfectly described by the *Cmca* unit cell, in which H atoms fill two types of sites, inside the deformed octahedral Mg_4Ni_2 site and in the infinite bended spirals –Ni–H–Ni–H– penetrating through the structure.

The DFT calculations showed that the *Cmca* phase of $MgNi_2H_3$ is the most stable one among all considered alternatives, both from the electronic structure and the lattice dynamics arguments. Quasi-harmonic phonon calculations allowed estimating the heat capacity of the tri-hydride $MgNi_2H_3$. The Bader charge analysis for $MgNi_2H_3$ indicates an electronic transfer from Mg ($-1.59e^-$) to Ni ($+0.21e^-$), H1 ($+0.55e^-$) and H2 ($+0.31e^-$). The phonon dispersion curves of $MgNi_2H_3$ all show positive frequencies, indicating that the structure is mechanically stable. The calculated gross heat of formation of the *Cmca*-type $MgNi_2H_3$ is -37.3 kJ/mol-H_2, which makes it by 3 kJ/mol-H_2 more stable than the prototype structures tested earlier (Yartys et al. [1]). The stability of the crystal structure of $MgNi_2H_3$ is enhanced by the formation of the directional Ni–H covalent bonds supplemented by the electron transfer from Mg to both Ni and H atoms. Similar directional covalent Ni–H bonding has been observed earlier in the anisotropic $CeNi_3H_{2.7}$ [22] and $Ce_2Ni_7H_{4.7}$ [23] hydrides and it also led to a significant rebuilding of the metal sublattices [24]. Thus, a strong Ni–H bonding interaction appears to be a key feature causing the rebuilding of the metal lattice during the process of formation of ternary hydrides.

Acknowledgements

This work is partly based on experiments performed at the Swiss spallation neutron source SINQ, Paul Scherrer Institute, Villigen, Switzerland.

The work was supported by ERA Net Russia FP7 program (Project NOVELMAG # 225) and a Grant by the Program "Elementary Particle Physics, Fundamental Nuclear Physics and Nuclear Technologies" of the Russian Academy of Sciences.

DFT and phonon calculations were performed using HPC resources from GENCI – CINES/IDRIS (Grants 2015-096175 and 2015-090189).

References

[1] V.A. Yartys, V.E. Antonov, A.I. Beskrovnyy, J.-C. Crivello, R.V. Denys, V.K. Fedotov, M. Gupta, V.I. Kulakov, M.A. Kuzovnikov, M. Latroche, Yu.G. Morozov, S.G. Sheverev, B.P. Tarasov, Hydrogen-assisted phase transition in a trihydride $MgNi_2H_3$ synthesized at high H_2 pressures: Thermodynamics, crystallographic and electronic structures, Acta Mater. 82 (2015) 316–327.

[2] R. Kataoka, Y. Goto, A. Kamegawa, H. Takamura, Masuo Okada, High-pressure synthesis of novel hydride in Mg–Ni (–H) system, Mater. Trans. 47 (2006) 1957–1960.

[3] R. Kataoka, A. Kamegawa, H. Takamura, M. Okada, High pressure synthesis of novel $Mg(Ni_{1-x}Cu_x)_2$ hydrides ($x = 0$–0.2), Mater. Trans. 50 (2009) 1179–1182.

[4] V.A. Yartys, V.V. Burnasheva, V.A. Yartys, N.V. Fadeeva, S.P. Solov'ev, K.N. Semenenko, Crystal chemistry of $RT_2H(D)_x$, $RT_5H(D)_x$ and $RT_3H(D)_x$ hydrides based on intermetallic compounds of $CaCu_5$, $MgCu_2$, $MgZn_2$ and $PuNi_3$ structure types, Int. J. Hydrogen Energy 7 (1982) 957–965.

[5] V.E. Antonov, Phase transformations, crystal and magnetic structures of high-pressure hydrides of d-metals, J. Alloys Compd. 330–332 (2002) 110–116.

[6] L.G. Khvostantsev, V.N. Slesarev, V.V. Brazhkin, Toroid type high-pressure device: history and prospects, High Pressure Res. 24 (2004) 371–383.

[7] H. Brian Toby, EXPGUI, a graphical user interface for GSAS, J. Appl. Crystallogr. 34 (2001) 210–213.

[8] P.E. Blöchl, Projector augmented-wave method, Phys. Rev. B 50 (1994) 17953–17979.

[9] G. Kresse, J. Furthmüller, Efficient iterative schemes for ab initio total-energy calculations using a plane-wave basis set, Phys. Rev. B 54 (1996) 11169–11186.

[10] G. Kresse, D. Joubert, From ultrasoft pseudopotentials to the projector augmented-wave method, Phys. Rev. B 59 (1999) 1758–1775.

[11] J.P. Perdew, K. Burke, M. Ernzerhof, Emission in symmetric heavy ion reactions at subthreshold energies, Phys. Rev. Lett. 78 (1997) 1396–1399.

[12] L. Chaput, A. Togo, I. Tanaka, G. Hug, Phonon-phonon interactions in transition metals, Phys. Rev. B 84 (2011) 094302.

[13] K. Parlinski, Z.Q. Li, Y. Kawazoe, First-principles determination of the soft mode in cubic ZrO_2, Phys. Rev. Lett. 78 (1997) 4063–4066.

[14] A. Togo, F. Oba, I. Tanaka, First-principles calculations of the ferroelastic transition between rutile-type and $CaCl_2$-type SiO_2 at high pressures, Phys. Rev. B 78 (2008) 134106.

[15] R.F.W. Bader, N. York (Eds.), Atoms in molecules: a quantum theory, Oxford University Press, Oxford, 1990.

[16] G. Henkelman, A. Arnaldsson, H. Jónsson, A fast and robust algorithm for Bader decomposition of charge density, Comput. Mater. Sci. 36 (2006) 354–360.

[17] R.V. Denys, V.A. Yartys, Colin J. Webb, Hydrogen in $La_2MgNi_9D_{13}$: the role of magnesium, Inorg. Chem. 51 (2012) 4231–4238.

[18] J.F. Herbst, L.G. Hector Jr., Structural discrimination via density functional theory and lattice dynamics: monoclinic Mg_2NiH_4, Phys. Rev. B 79 (2009) 155113.

[19] B. Dorner, I.T. Belash, E.L. Bokhenkov, E.G. Ponyatovsky, V.E. Antonov, L.N. Pronina, Inelastic incoherent neutron scattering spectra from fcc $NiH_{1.05}$, hcp $CrH_{1.0}$ and hcp $MoH_{1.2}$ at 15 K, Solid State Commun. 69 (1989) 121–124.

[20] J. Wollam, E. Wallace, Magnetic susceptibility, heat capacity and third-law entropy of $MgNi_2$, J. Phys. Chem. Solids 13 (1960) 212–220.

[21] H. Feufel, F. Sommer, Thermodynamic investigations of binary liquid and solid Cu–Mg and Mg–Ni alloys and ternary liquid Cu–Mg–Ni alloys, J. Alloys Compd. 224 (1995) 42–54.

[22] V.A. Yartys, O. Isnard, A.B. Riabov, L.G. Akselrud, Unusual effects of hydrogenation: anomalous expansion and volume contractions, J. Alloys Compd. 356–357 (2003) 109–113.

[23] R.V. Denys, V.A. Yartys, Masashi Sato, A.B. Riabov, R.G. Delaplane, Crystal chemistry and thermodynamic properties of anisotropic $Ce_2Ni_7H_{4.7}$ hydride, J. Solid State Chem. 180 (2007) 2566–2576.

[24] V.A. Yartys, P. Vajeeston, A.B. Riabov, P. Ravindran, R.V. Denys, J.P. Maehlen, R.G. Delaplane, H. Fjellvåg, Crystal chemistry and metal-hydrogen bonding in anisotropic and interstitial hydrides of intermetallics of rare earth (R) and transition metals (T), RT_3 and R_2T_7, Z. Kristallogr. 223 (2008) 674–689.